

The detection and treatment of distance errors in kinematic analyses of stars

Ralph Schönrich^{1*}, James Binney² and Martin Asplund¹

¹ *Max Planck Institute for Astrophysics, Karl-Schwarzschild-Str. 1, D-85741 Garching*

² *University of Oxford, Rudolf-Peierls Centre for Theoretical Physics, Keble Road, Oxford OX1 3NP*

October 28th, 2011

ABSTRACT

We present a new method for detecting and correcting systematic errors in the distances to stars when both proper motions and line-of-sight velocities are available. The method, which is applicable for samples of 200 or more stars that have a significant extension on the sky, exploits correlations between the measured U , V and W velocity components that are introduced by distance errors. We deliver a formalism to describe and interpret the specific imprints of distance errors including spurious velocity correlations and shifts of mean motion in a sample. We take into account correlations introduced by measurement errors, Galactic rotation and changes in the orientation of the velocity ellipsoid with position in the Galaxy. Tests on pseudodata show that the method is more robust and sensitive than traditional approaches to this problem. We investigate approaches to characterising the probability distribution of distance errors, in addition to the mean distance error, which is the main theme of the paper. Stars with the most overestimated distances bias our estimate of the overall distance scale, leading to the corrected distances being slightly too small. We give a formula that can be used to correct for this effect. We apply the method to samples of stars from the SEGUE survey, exploring optimal gravity cuts, sample contamination, and correcting the used distance relations.

Key words: stars: distances - statistics - kinematics - fundamental parameters
Galaxy: structure - kinematics and dynamics

1 INTRODUCTION

Studies of stellar kinematics in the Milky Way are of enormous importance as they hold the key both to measuring the gravitational field of the Galaxy and to unravelling the Galaxy’s history and manner of formation. Consequently considerable resources have been, and are being, devoted to measuring the velocities of stars.

Two different techniques have to be used to measure the three components of velocity with respect to the Sun: the component v_{\parallel} along the line of sight to the star is measured spectroscopically, while the component \mathbf{v}_{\perp} transverse to the line of sight is determined by combining the measured proper motion μ with an estimate of the distance s to the star. Over the next decade enormous numbers of distances will be obtained from parallaxes measured by the Gaia satellite, but currently the great majority of distance estimates have been obtained by comparing an estimate of the star’s absolute magnitude with its apparent magnitude. This process

is liable to systematic error in several ways. Giants can be mistaken for subgiants or even dwarfs of the same colour (or vice versa) and assumed ages severely influence the adopted luminosities in the turn-off region even for well classified stars. Also, the adopted metallicities may be biased as discussed by Lee et al. (2008a) and as demonstrated by the shifts in metallicity scale between Nordström et al. (2004), Holmberg et al. (2007) and Casagrande et al. (2011). An erroneous metallicity will lead to the wrong isochrone being used to infer the luminosity, and an erroneous luminosity and distance will follow. Further problems are that synthetic colours can be wrong (cf. the discussion in Percival & Salaris 2009) and that stellar-evolution models can predict different luminosities for given metallicity and effective temperatures; there is evidence that they make the main sequences of metal-poor objects too faint (the “helium problem”, e.g. discussed in Casagrande et al. 2007). Finally, erroneous extinctions may be adopted. Since the problems just enumerated can readily accumulate to systematic distance biases in excess of 20 per cent, some way of independently calibrating the distance scale is invaluable.

* E-mail: rasch@mpa-garching.mpg.de

Here we present a method for calibrating distances that exploits correlations between the measured U, V, W components of velocity that are introduced by systematic distance errors, and is applicable to any survey that provides proper motions and line-of-sight velocities over a wide area of the sky.

The idea that the typical distance to objects in a sample can be constrained by proper motions is well known in astronomy – for a useful recent review see Popowski & Gould (1998). The method of secular parallaxes determines the mean parallax of a population by combining proper motions and the known mean motion of the population with respect to the Sun (e.g. Trumpler & Weaver 1962; Binney & Merrifield 1998, §2.2.3), while the method of statistical parallaxes estimates the mean parallax by combining proper motions with line-of-sight velocities (e.g. Binney & Merrifield 1998, §2.2.4). Our method has points in common with both the above methods in that it hinges on comparing proper motions with line-of-sight velocities but also exploits the mean motion of the stars with respect to the Sun. It is much less vulnerable than classical methods to questionable assumptions regarding the shape of the velocity ellipsoid and/or the nature of mean velocity field (see esp. the discussion in Trumpler & Weaver 1962). By examining the way correlations between components of space velocity vary with position on the sky, we dispense with the need for prior knowledge of the mean velocity field. All we require is knowledge of the formal errors of the observables and, if the sample is sufficiently non-local, reasonable assumptions about the orientation of the velocity ellipsoid at relevant points in the Galaxy.

Section 2 lays out the basic theory for the case in which distances are all in error by a common factor. Section 3 extends the theory to the realistic case in which distance errors contain a random component. Section 4 applies the method to data from the Sloan surveys. Section 5 sums up.

2 THE MEAN DISTANCE ERROR

We are concerned with the case in which calibration errors in the distance scale cause all distances have a fractional error f , so the assumed distance s' to a star is related to the true distance s by

$$s' = (1 + f)s. \quad (1)$$

Consequently the assumed tangential velocity \mathbf{v}'_{\perp} is related to the true tangential velocity \mathbf{v}_{\perp} by

$$\mathbf{v}'_{\perp} = (1 + f)\mathbf{v}_{\perp}. \quad (2)$$

The velocity component v_{\parallel} along the line of sight is of course unaffected by distance errors.

From v_{\parallel} and the proper motions ($\mu_b = \dot{b}, \mu_l = \cos b \dot{l}$) parallel to each Galactic coordinate we infer the velocity components (U, V, W) in the Cartesian coordinate system in which the Sun is at rest at the origin. In this system the U axis points to the Galactic centre, the V axis points in the direction of Galactic rotation, and the W axis points to the north Galactic pole. The relevant transformation is

$$\begin{pmatrix} U_0 \\ V_0 \\ W_0 \end{pmatrix} = \mathbf{M} \begin{pmatrix} s\mu_b \\ s\mu_l \\ v_{\parallel} \end{pmatrix}, \quad (3)$$

where the orthogonal matrix

$$\mathbf{M} \equiv \begin{pmatrix} -\sin b \cos l & -\sin l & \cos b \cos l \\ -\sin b \sin l & \cos l & \cos b \sin l \\ \cos b & 0 & \sin b \end{pmatrix}. \quad (4)$$

The velocity components inferred from distances that have fractional error f are

$$\begin{pmatrix} U \\ V \\ W \end{pmatrix} = \mathbf{M}(\mathbf{I} + f\mathbf{P}) \begin{pmatrix} s\mu_b \\ s\mu_l \\ v_{\parallel} \end{pmatrix}, \quad (5)$$

where \mathbf{I} is the identity matrix and

$$\mathbf{P} \equiv \begin{pmatrix} 1 & 0 & 0 \\ 0 & 1 & 0 \\ 0 & 0 & 0 \end{pmatrix}. \quad (6)$$

Hence the true and measured Galactocentric components of velocity are related by

$$\begin{pmatrix} U \\ V \\ W \end{pmatrix} = \mathbf{M}(\mathbf{I} + f\mathbf{P})\mathbf{M}^T \begin{pmatrix} U_0 \\ V_0 \\ W_0 \end{pmatrix} = (\mathbf{I} + f\mathbf{T}) \begin{pmatrix} U_0 \\ V_0 \\ W_0 \end{pmatrix}, \quad (7)$$

where

$$\mathbf{T} \equiv \mathbf{M}\mathbf{P}\mathbf{M}^T. \quad (8)$$

Table 1 gives an explicit expression for \mathbf{T} , which has direction-dependent off-diagonal elements. Consequently, when $f \neq 0$ the inferred value of W has linear dependencies on U_0 and V_0 with coefficients that are known functions of Galactic position times f . By detecting these patterns of bias, we can measure the amount f by which distances have been overestimated.

The phenomenon we exploit can be understood by an example. Consider a star at a Galactic longitude $l = 0$ and latitude $b = 45^\circ$. Suppose the star's only non-zero component of velocity (in the Sun's rest frame) is $U_0 > 0$. This motion generates both a proper motion $\mu_b < 0$ and a line-of-sight velocity v_{\parallel} away from us. If we overestimate the star's distance, the tangential velocity, which lies in the (U, W) plane, will be overestimated, and we will infer a negative value for W instead of zero. By the same token, a star with overestimated distance that had $U_0 < 0$ would have $W > 0$. In the southern Galactic hemisphere signs reverse and a star with overestimated distance at $b = -45^\circ$ with $U_0 > 0$ will be wrongly assigned a positive value of W . Hence a systematic tendency to misjudge distances can be detected by looking for correlations between velocity components that vary over the sky in given ways.

The Sun moves in the direction of Galactic rotation faster than the circular speed and all Galactic components are subject to at least some asymmetric drift, so $\langle V_0 \rangle < 0$ for most groups of stars, especially halo stars. Consequently, the clearest signals of an erroneous distance scale are usually correlations between the measured values of U and V and between W and V .

2.1 A naive Approach

Equations (7) yield

$$\begin{aligned} U &= (1 + fT_{UU})U_0 + fT_{UV}V_0 + fT_{UW}W_0 \\ V &= (1 + fT_{VV})V_0 + fT_{VU}U_0 + fT_{VW}W_0 \\ W &= (1 + fT_{WW})W_0 + fT_{WU}U_0 + T_{WV}V_0. \end{aligned} \quad (9)$$

Table 1. Explicit expression for the matrix \mathbf{T} through which distance errors introduce correlations between the apparent components of velocity, and an expression for the relation between the errors in (U, V, W) and in (μ, v_{\parallel}) .

$$\mathbf{T} = \mathbf{M}\mathbf{P}\mathbf{M}^T = \begin{pmatrix} 1 - \cos^2 b \cos^2 l & -\frac{1}{2} \cos^2 b \sin 2l & -\frac{1}{2} \sin 2b \cos l \\ -\frac{1}{2} \cos^2 b \sin 2l & 1 - \cos^2 b \sin^2 l & -\frac{1}{2} \sin 2b \sin l \\ -\frac{1}{2} \sin 2b \cos l & -\frac{1}{2} \sin 2b \sin l & \cos^2 b \end{pmatrix}$$

$$\begin{pmatrix} e_U \\ e_V \\ e_W \end{pmatrix} = \mathbf{M}(\mathbf{I} + f\mathbf{P}) \begin{pmatrix} s\epsilon_b \\ s\epsilon_l \\ \epsilon_{\parallel} \end{pmatrix} = \begin{pmatrix} -\sin b \cos l(1+f)s\epsilon_b - \sin l(1+f)s\epsilon_l + \cos b \cos l\epsilon_{\parallel} \\ -\sin b \sin l(1+f)s\epsilon_b + \cos l(1+f)s\epsilon_l + \cos b \sin l\epsilon_{\parallel} \\ \cos b(1+f)s\epsilon_b + \sin b\epsilon_{\parallel} \end{pmatrix}$$

Suppose for each hemisphere $b > 0$ and $b < 0$ we bin stars in l and in $V \simeq V_0$. Then for each bin we could average the first and third equations, obtaining for each bin two equations

$$\begin{aligned} \langle U \rangle &= \langle (1 + fT_{UU})U_0 \rangle + f\langle T_{UV}V_0 \rangle + f\langle T_{UW}W_0 \rangle \\ \langle W \rangle &= \langle (1 + fT_{WW})W_0 \rangle + f\langle T_{WU}U_0 \rangle + f\langle T_{WV}V_0 \rangle. \end{aligned} \quad (10)$$

We expect the population of stars under study, taken as a whole, to be moving neither radially nor vertically, so at any (b, l) the mean values of U_0 and W_0 should be the reflex of the solar motion, (U_{\odot}, W_{\odot}) . With this assumption in the U equation we may set

$$\begin{aligned} \langle (1 + fT_{UU})U_0 \rangle &= -(1 + f\langle T_{UU} \rangle)U_{\odot} \\ \langle T_{UW}W_0 \rangle &= -\langle T_{UW} \rangle W_{\odot}, \end{aligned} \quad (11)$$

and similar relations can be used in the W equation. Finally we make f the only unknown in equations (10) by assuming, in a first approximation, that $V_0 = V$. On account of Poisson noise, the sample values of quantities such as $\langle T_{UW}W_0 \rangle$ will differ from our adopted value, $-\langle T_{UW} \rangle W_{\odot}$, so the equations will not be exactly satisfied, but we can seek the values of f that minimise the quantities

$$\begin{aligned} S'_U &\equiv \sum_{\text{bins}} [\langle U \rangle + (1 + f\langle T_{UU} \rangle)U_{\odot} \\ &\quad - f\langle T_{UV}V \rangle + f\langle T_{UW} \rangle W_{\odot}]^2 \\ S'_W &\equiv \sum_{\text{bins}} [\langle W \rangle + (1 + f\langle T_{WW} \rangle)W_{\odot} \\ &\quad + f\langle T_{WU} \rangle U_{\odot} - f\langle T_{WV}V \rangle]^2. \end{aligned} \quad (12)$$

After determining the optimum value of f , this value can be used to correct the distances and the velocities derived from them, and a new value of f is then obtained, enabling the distances to be corrected a second time, and so on until convergence has been reached.

The scheme just described is straightforward conceptually and does work, but suffers a significant loss of information from the need to bin the data and to replace the measured values of U and W by $-U_{\odot}$ and $-W_{\odot}$. Therefore the results shown in this paper are obtained by a different scheme that is described in the next subsection.

2.2 A more effective approach

Our method is based on the principle that the true value of U or W can be decomposed into a mean velocity field of known form with components \bar{U} and \bar{W} , plus a random variable δU or δW that has zero mean, so $U_0 = \bar{U} + \delta U$, etc. In this subsection we make the assumption that the mean velocity field may be approximated by the reflex of the solar motion, so $\bar{U} = -U_{\odot}$ etc. In Section 2.5.1 we will lift this

restriction to allow for Galactic rotation. Also we argue that in the second or third terms on the right of equations (9) we may replace V_0 by V on the ground that the inferred value is close to the true value and the presence in these terms of an explicit factor f implies that the error made by replacing V_0 by V is $O(f^2)$. The same argument enables us to replace U_0 by U and W_0 by W in these terms. With these replacements the first and third of equations (9) become

$$\begin{aligned} U &= -U_{\odot} + fx + (1 + fT_{UU})\delta U \\ W &= -W_{\odot} + fy + (1 + fT_{WW})\delta W, \end{aligned} \quad (13)$$

where

$$\begin{aligned} x &\equiv -T_{UU}U_{\odot} + T_{UV}V + T_{UW}W \\ y &\equiv -T_{WW}W_{\odot} + T_{WU}U + T_{WV}V. \end{aligned} \quad (14)$$

We now eliminate reliance on prior knowledge of the solar motion by subtracting from each of equations (13) its expectation value, and have

$$\begin{aligned} U - \langle U \rangle &= f(x - \langle x \rangle) + (1 + fT_{UU})\delta U \\ W - \langle W \rangle &= f(y - \langle y \rangle) + (1 + fT_{WW})\delta W, \end{aligned} \quad (15)$$

We determine the optimum value of f by forming the sample sums¹

$$\begin{aligned} \sum_i [U_i - \langle U \rangle - f(x_i - \langle x \rangle)]x_i &= \sum_i (1 + fT_{UU})\delta U_i x_i \\ \sum_i [W_i - \langle W \rangle - f(y_i - \langle y \rangle)]y_i &= \sum_i (1 + fT_{WW})\delta W_i y_i. \end{aligned} \quad (16)$$

The right side of the first equation would vanish if δU were uncorrelated with x but it *is* correlated because x depends on V and W , which in turn depend on $U_0 = -U_{\odot} + \delta U$. In fact one easily shows that

$$\langle (1 + fT_{UU})\delta U x \rangle = f\langle (1 + fT_{UU})(T_{UV}^2 + T_{UW}^2)\delta U^2 \rangle. \quad (17)$$

Since we are working to $O(f)$ only, we neglect the second term in the first bracket on the right and use the resulting expression in equation (16) to solve for f . We find

$$f = \frac{\text{Cov}(U, x)}{\text{Var}(x) + \langle T_{UV}^2 + T_{UW}^2 \rangle \sigma_U^2}, \quad (18)$$

where $\sigma_U^2 \equiv \langle \delta U^2 \rangle$ and we have identified sample means with expectation values. Analogously, from the second of equations (16) we have

¹ The accuracy with which f is determined can be slightly increased by weighting each term in the sums in eqs.(16) by the inverse of the expected standard deviation of the noise term or by using Huber-White standard errors (White 1980).

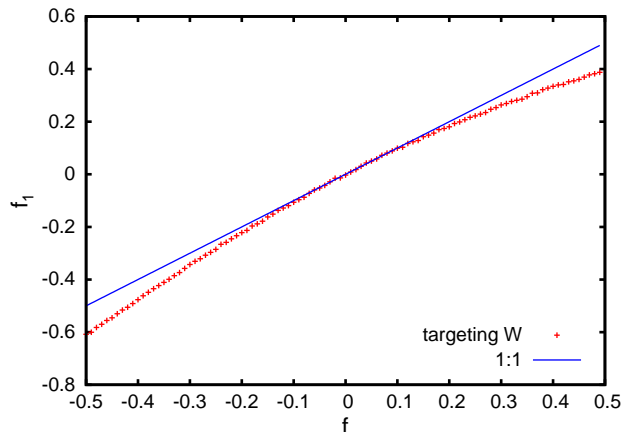


Figure 1. Value of the fractional distance error f_1 from equation (19) versus value of f bias in a mock sample of 450 000 disc and 50 000 halo stars. The blue line has unit slope.

Table 2. Parameters of the mock disc and halo samples used in tests. All velocities are in km s^{-1}

Component	σ_U	σ_V	σ_W	\bar{v}_ϕ
Disc	55	45	35	180
Halo	150	75	75	0

$$f = \frac{\text{Cov}(W, y)}{\text{Var}(y) + \langle T_{WV}^2 + T_{WU}^2 \rangle \sigma_W^2}. \quad (19)$$

As with the naive scheme, we proceed iteratively, successively correcting the distances according to the value of f yielded by the current distances, until f becomes negligible. The precise values of the denominators in our expressions for f are not important because we rescale distances until $f \propto \text{Cov}(U, x) = 0$ or $f \propto \text{Cov}(W, y) = 0$. This circumstance is fortunate as only an approximate values of σ_U and σ_W may be available. Note that equations (18) and (19) make no reference to the solar motion so that in contrast to the secular parallax they require only information about the shape, but not the average value of the mean velocity field.

In the following, when using equation (18) we shall call U the “target variable” and x the “explaining variable”, while when we use equation (19), W will be the target variable and y the explaining variable.

The reader may wonder why we do not obtain a third estimate of f from the V equation of the set (9). The problem is that we cannot write $V_0 = -V_\odot + \delta V$ by analogy with our treatment of U and W , because most stellar groups have mean azimuthal velocities smaller than that of the Sun, and in fact the mean azimuthal velocity of a group will vary with location.

The quantities $\sum_i U_i x_i$ and $\sum_i W_i y_i$ implicit in the right sides of equations (18) and (19) contain cross-terms such as $\sum_i U_i V_i$ and $\sum_i U_i W_i$. As explained above, usually the V cross-terms contain the largest amount of information regarding f , except when V lies near zero, when the W cross-terms provide the strongest constraints on f . W is the target velocity of choice both because it has the lowest velocity dispersion, and because it is least affected by streaming motions, which are largely confined to the UV plane (Dehnen 1998).

2.3 Tests

In this section we test the effectiveness of the scheme derived in the last subsection by deriving pseudo-data from a model Galaxy, and analysing them in the presence of systematic distance errors. We have conducted such tests using a model obtained by adding gas and star formation to a halo formed in simulations of the cosmological clustering of collisionless particles. The results of these tests were entirely satisfactory, but we do not report them here for two reasons: (a) considerable space would be required to describe the Galaxy model with sufficient precision and the model is in any case not entirely realistic, and (b) the model provides a rather limited number of particles in the vicinity of the Sun, so the statistical precision of the tests is inferior to that of the tests we will present. These use data obtained from a Galaxy model that is highly idealised, but which has the flexibility to produce data that include or exclude whatever features in the data might affect the performance of our method.

Our idealised Galaxy model has a non-rotating halo and a rotating disc. The velocity ellipsoids of both components are triaxial Gaussians: Table 2 gives the values of the dispersions. The mean rotation velocity of the disc is taken to be 180 km s^{-1} and the circular speed is 220 km s^{-1} . The sampled stars are distributed uniformly in distance between 0.5 kpc and 4 kpc, and uniformly in Galactic longitude and latitude, which gives the sample a strong poleward bias that resembles the bias encountered in real samples better than an isotropically distributed sample would. The solar motion is in addition offset by the local standard of rest velocity vector as determined by Schönrich et al. (2010).

The crosses in Fig. 1 show the value of f recovered from equation (19) on the first iteration, f_1 , versus the preset fractional distance overestimate f applied to the sample. Each cross shows an independent realisation of the pseudo-data, which contained 450 000 disc and 50 000 halo stars. The crosses fall on a curve that passes through (0, 0) as we would hope. The straight line through the origin with unit slope is also plotted and we see that for $|f| \lesssim 0.2$ the slope of the curve is close to unity, so convergence of the iterative procedure is rapid. However, the key point is that the curve passes through the origin and has no point of inflection. So long as these conditions are satisfied, the iterative scheme will converge on the correct distance scale regardless of the slope or curvature of the curve.

Fig. 2 demonstrates that the method works well even in the absence of solar motion by showing results analogous to those of Fig. 1 for a sample of stars that has no net motion with respect to the Sun and an isotropic velocity distribution around the solar motion, i.e. without any systematic offset. The minor difference between the estimators on U and W derives from second-order effects in f by the polewards bias in the sample geometry. Note that a simple linear regression of W on y from equation (13) would give the right zero point and so finally an unbiased distance estimate, but due to the lack of correction factors to the denominator $\text{Var}(x)$ would give a slope that is a factor 2 too large and hence a bad convergence behaviour in the iteration.

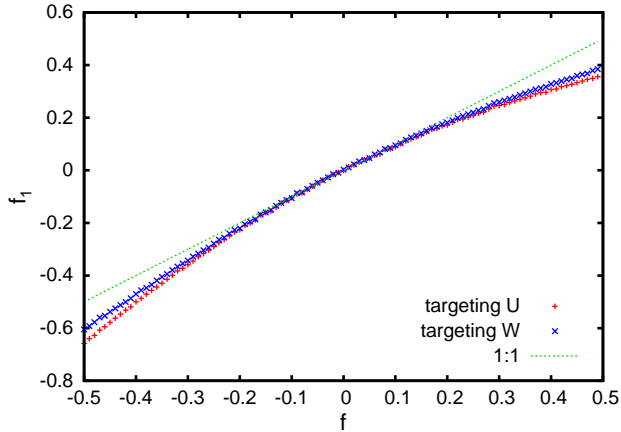


Figure 2. Value of the fractional distance error f from equation (18) or (19) versus the input value of f for samples of 500 000 stars with an isotropic velocity distribution and no solar motion. The line of unit slope is also shown.

2.4 Impact of random errors

We now consider the impact on our technique of random measurement errors. If we measured U , V and W directly, random errors would have no impact because they would simply inflate the scatter in these variables that is inherent in stars having random velocities. Unfortunately, we do not measure U , V , W directly but calculate them from the measured values of μ_b , μ_l and v_{\parallel} . Consequently the error in say μ_l introduces correlated errors into both U and V . Since our technique consists precisely in attributing correlations between U and x (which depends on V) to a non-zero value of f , we must consider the contribution of the errors to the correlations between U and x or W and y if we are to estimate f correctly.

Our key assumption is that the errors in μ_b , μ_l and v_{\parallel} are statistically independent, have vanishing mean, and have finite and approximately known variances. Let ϵ_b , ϵ_l , ϵ_{\parallel} be the errors in the proper motions and line-of-sight velocity. Then the random errors in U , V , W are

$$\begin{pmatrix} e_U \\ e_V \\ e_W \end{pmatrix} = \mathbf{M}(\mathbf{I} + f\mathbf{P}) \begin{pmatrix} s\epsilon_b \\ s\epsilon_l \\ \epsilon_{\parallel} \end{pmatrix}. \quad (20)$$

Table 1 gives an explicit expression for the right side of this equation.

Consider now the correlation, between a target variable, say W , and the explaining variable y . Let $W = W' + e_W$ and $y = y' + e_y$, where the primed variables are the components without the error and e_W , e_y are their errors derived from equation (20)

$$\langle Wy \rangle = \langle W'y' \rangle + \langle e_W e_y \rangle + \langle W'e_y \rangle + \langle e_W y' \rangle. \quad (21)$$

Given that the errors are unbiased, the correlations such as $\langle W'e_y \rangle$ between the true velocities and the errors vanish. Consequently the changes in f that the errors introduce through equation (19) is

$$e_f = \frac{\langle e_W e_y \rangle}{\langle y^2 \rangle + \langle T_{WU}^2 + T_{WV}^2 \rangle \sigma_W^2} - f \frac{\langle e_y^2 \rangle}{\langle y^2 \rangle + \langle T_{WU}^2 + T_{WV}^2 \rangle \sigma_W^2}. \quad (22)$$

The second term on the right side is smaller than the first, and as we iterate towards $f = 0$ it vanishes altogether. Hence we neglect it. With this term neglected, we can obtain the error-corrected value of f simply by subtracting $\langle e_W e_y \rangle$ from the measured value of $\langle Wy \rangle$ before inserting its value into equation (19).

We now calculate the error-error correlations. We have from equations (14)

$$\begin{aligned} \langle e_U e_x \rangle &= T_{UV} \langle e_U e_V \rangle + T_{UW} \langle e_U e_W \rangle \\ \langle e_W e_y \rangle &= T_{WU} \langle e_W e_U \rangle + T_{WV} \langle e_W e_V \rangle. \end{aligned} \quad (23)$$

When we use Table 1 to express the errors in terms of the (uncorrelated) errors in the observables, we find

$$\begin{aligned} \langle e_U e_V \rangle &= \frac{1}{2} \sin 2l [(1+f)^2 s^2 (\sin^2 b \epsilon_b^2 - \epsilon_l^2) + \cos^2 b \epsilon_{\parallel}^2] \\ \langle e_U e_W \rangle &= -\frac{1}{2} \sin 2b \cos l [(1+f)^2 s^2 \epsilon_b^2 - \epsilon_{\parallel}^2] \\ \langle e_W e_V \rangle &= -\frac{1}{2} \sin 2b \sin l [(1+f)^2 s^2 \epsilon_b^2 - \epsilon_{\parallel}^2]. \end{aligned} \quad (24)$$

From the definition of f we see that these terms exclusively depend on the measured distance $s' = (1+f)s$, so we can correct for proper-motion errors before determining f . Finally using the explicit form of \mathbf{T} from Table 1 we obtain our correction terms:

$$\begin{aligned} \langle e_U e_x \rangle &= -\frac{1}{4} \{ \cos^2 b \sin^2 2l [(s'^2 (\sin^2 b \epsilon_b^2 - \epsilon_l^2) + \cos^2 b \epsilon_{\parallel}^2) \\ &\quad - \sin^2 2b \cos^2 l [s'^2 \epsilon_b^2 - \epsilon_{\parallel}^2]] \} \\ \langle e_W e_y \rangle &= \frac{1}{4} \sin^2 2b \{ s'^2 \epsilon_b^2 - \epsilon_{\parallel}^2 \}. \end{aligned} \quad (25)$$

The left panels in Fig. 3 show $\langle e_W e_y \rangle$ as a function of the errors in the line-of-sight velocities (upper panel) and the errors in proper motions (lower panel). (In the upper panels the proper-motion data are error-free, while in the lower panels the line-of-sight velocities are error-free.) All points are determined from realisations of a Monte-Carlo sample of 450 000 disc stars and 50 000 halo stars sampled from the model described by Table 2. The agreement between the analytic formula and the Monte-Carlo results is perfect. On account of the large distances of most of the stars, the proper-motion errors produce substantially greater values of $\langle e_W e_y \rangle$ than do the errors in v_{\parallel} (which will be negligible for most present-day samples). The right panels of Fig. 3 show the shifts in f_1 (red crosses) that arise from the correlations plotted on the left. The uncorrected values of f_1 exhibit a quadratic behaviour for small errors as can be expected from equation (25), while for larger errors growth in the denominator on the right of equation (19) abates the growth in $|f_1|$. The blue crosses show the values for f_1 obtained when we correct our estimate according to equation (25). The green squares in the bottom right panel depict the case when we vary σ_{μ_b} at a fixed line-of-sight velocity error $\sigma_{v_{\parallel}} = 30 \text{ km s}^{-1}$. This demonstrates that the error effects can be added linearly and our formalism gives a perfect account of them (purple circles). We also checked that as predicted σ_{μ_l} does not affect our distance estimate when targeting W .

The largest uncertainty in the corrections given by equations (25) lies in the assessment of the measurement errors. The model data used above include remote disc stars, which have errors that are larger than will often be encountered in practice. So this test suggests that it should be possible to correct for the effects of measurement errors in most samples.

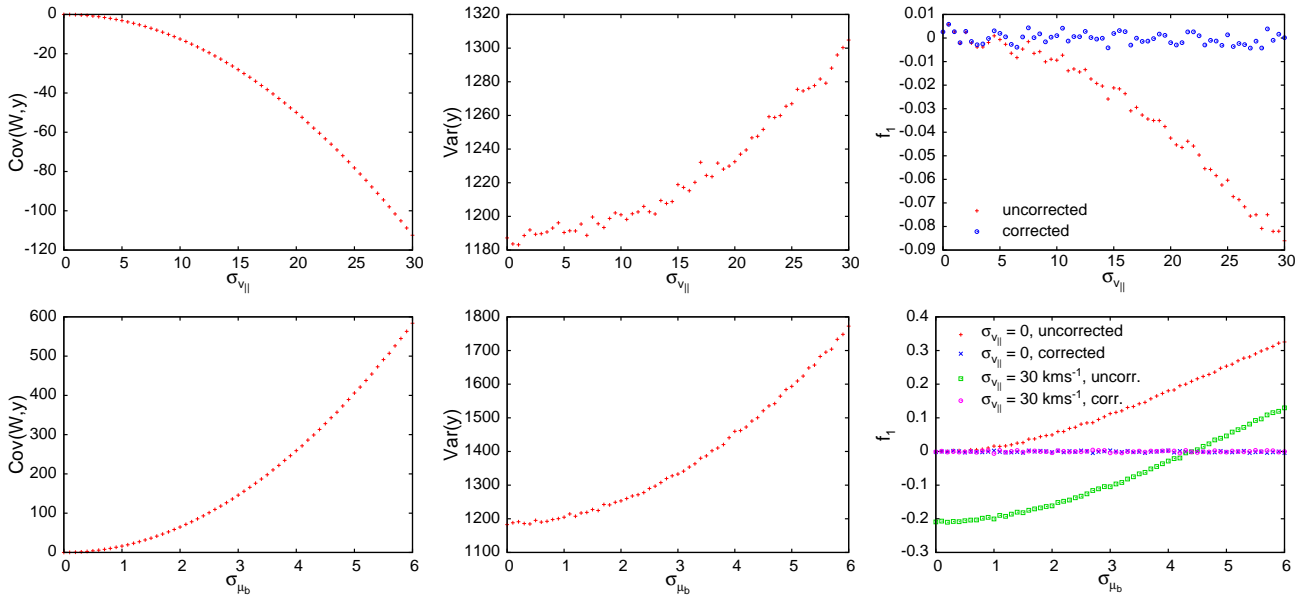


Figure 3. Tests of the effects of random measurement errors in a mock sample of 500 000 stars, among which are 50 000 halo stars. The left and centre panels show how the values of $\text{Cov}(W, y)$ and $\text{Var}(y)$ are affected by measurement errors, while the right panels show the values of f_1 using equation(19) with and without the correction terms for these samples. In the upper row the proper motions are error free and the horizontal axis gives the error in v_{\parallel} , while in the lower panel v_{\parallel} is error free (red and green crosses) and the horizontal axis gives the error in proper motions. In the bottom right panel we added the case of a fixed radial velocity error of 30 km s^{-1} (green squares and purple circles) to demonstrate the simple superposition of the error correlation terms on the covariance.

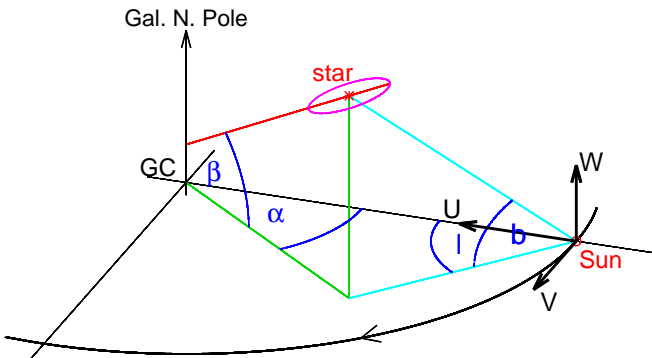


Figure 4. The definition of Galactic coordinates, heliocentric velocities and the angles α and β . GC signifies the Galactic Centre. The purple ellipse depicts the direction of the radially oriented main axis of the velocity ellipsoid (along U_g), which defines β .

2.5 Rotation of the velocity ellipsoid

Regardless of a star's location, we have been decomposing its velocity into Cartesian components in the frame that is aligned with the Sun-centre line. Since this frame is not aligned with the principal axes of the velocity ellipsoid at the location of a distant star, we anticipate non-vanishing values of $\langle UV \rangle$, etc., even in the absence of distance errors. We now address this issue.

Let the components of velocity of any star along the principal axes of its local velocity ellipsoid be (U_g, V_g, W_g) . Then with the angles α and β defined as shown in Fig. 4, the angle α between the projection onto the plane of the

velocity ellipsoid's long axis and the Sun-centre line is given by

$$\alpha = \arctan \left(\frac{s \sin l \cos b}{R_0 - s \cos l \cos b} \right), \quad (26)$$

and the heliocentric velocity components (U, V, W) are given by

$$\begin{pmatrix} U + U_{\odot} \\ V + V_{\odot} \\ W + W_{\odot} \end{pmatrix} = \mathbf{R}(\alpha, \beta) \begin{pmatrix} U_g \\ V_g \\ W_g \end{pmatrix}, \quad (27)$$

where

$$\mathbf{R}(\alpha, \beta) \equiv \begin{pmatrix} \cos \alpha \cos \beta & \sin \alpha & \cos \alpha \sin \beta \\ -\sin \alpha \cos \beta & \cos \alpha & -\sin \alpha \sin \beta \\ -\sin \beta & 0 & \cos \beta \end{pmatrix}. \quad (28)$$

Both observation (Siebert et al. 2011) and theory (Binney & McMillan 2011) suggest that α and β will take values close to the Galactocentric azimuth ϕ and latitude $\frac{1}{2}\pi - \theta$ of the location in question. In our tests we will assume that these relations are exact.

2.5.1 Correlations from mean streaming

A major contribution to the velocity components U and V comes from the azimuthal streaming of stars, which we take to have magnitude $\bar{v}_{\phi}(R, z)$. This motion invalidates our assumption above that $U = -U_{\odot} + \delta U$. Instead we now have $U = -U_{\odot} + \bar{U} + \delta U$, where \bar{U} is the U component of the velocity field given by \bar{v}_{ϕ} at the star's location. Specifically we have

$$\bar{U}(s, l, b) = \bar{v}_{\phi} \sin \alpha, \quad (29)$$

where there is dependence on (s, l, b) both through α and through the (generally unknown) dependence of \bar{v}_{ϕ} on

(R, z) . Unfortunately, both T_{UV} and \bar{U} are odd functions of l , so correlations contributed by distance errors can be interpreted as due to differential rotation and vice versa. On account of this fact, W , to which \bar{v}_ϕ does not contribute, is a more useful target velocity than U . However, it is nonetheless worthwhile to consider how U can be targeted.

The first of equations (13) now becomes

$$U = -U_\odot + \bar{v}_\phi \sin \alpha + f x' + (1 + f T_{UV}) \delta U. \quad (30)$$

To determine f from these equations we assume that

$$\bar{v}_\phi = \Theta g(R, z), \quad (31)$$

where $g(R, z)$ is a function that describes the way in which \bar{v}_ϕ varies with position and $\Theta \equiv \bar{v}_\phi(R_0, 0)$ is the local streaming velocity of the population under study. In the simplest case we assume that g has no dependence on R , and we estimate its dependence on z from the data, using the current distance scale. Once g has been chosen, and a preliminary value for Θ adopted, we can determine the value of x for each star. We primed x in equation (30) because x contains the mean motion in U , so we have to split off the rotation term:

$$x' = x + T_{UV} \Theta g(R, z) \sin \alpha. \quad (32)$$

The distance error f causes the measured α' to deviate from the true value α , but we can correct for this effect by Taylor-expanding $\alpha'(f)$:

$$\sin \alpha = \sin \alpha' - f \cos^3 \alpha' \frac{s' R_0 \sin l \cos b}{(R_0 - s' \cos l \cos b)^2} + O(f^2). \quad (33)$$

Then

$$U = -U_\odot + \Theta \rho + f x + f \Theta k + (1 + f T_{UV}) \delta U, \quad (34)$$

where

$$\rho \equiv g(R, z) \sin \alpha' \\ k \equiv T_{UV} \rho + \cos^3 \alpha' \frac{s' R_0 \sin l \cos b}{(R_0 - s' \cos l \cos b)^2}. \quad (35)$$

Now we can proceed identically to the derivation of equation (18): we first subtract from equation (34) its expectation value to obtain

$$U - \langle U \rangle - \Theta(\rho - \langle \rho \rangle) - f(x - \langle x \rangle) - f\Theta(k - \langle k \rangle) = (1 + f T_{UV}) \delta U, \quad (36)$$

and then we multiply x_i and ρ_i and sum over our sample. Introducing the abbreviation $s_{a,b} \equiv \text{Cov}(a, b)$, this gives two equations for the unknowns f and Θ :

$$s_{Ux} - \Theta s_{\rho x} - f s_{xx} - \Theta f s_{kx} = f \langle T_{UV}^2 + T_{UW}^2 \rangle \sigma_U^2 \\ s_{U\rho} - \Theta s_{\rho\rho} - f s_{\rho x} - \Theta f s_{k\rho} = 0 \quad (37)$$

Inserting Θ from the second equation into the first and dropping all terms of order f^2 we obtain our estimator

$$f = \frac{s_{Ux} s_{\rho\rho} - s_{\rho x} s_{U\rho}}{s_{xx} s_{\rho\rho} - s_{\rho x}^2 + s_{kx} s_{U\rho} - s_{Ux} s_{k\rho} + t^2 \sigma_U^2 s_{\rho\rho}} \quad (38)$$

where $t^2 \equiv \langle T_{UV}^2 + T_{UW}^2 \rangle$. For a quick calculation the third and fourth term in the denominator can be neglected as they are in general small and only affect the slope. Again we solve these equations iteratively, at each iteration updating the distances and recalculating for each star x , α and g .

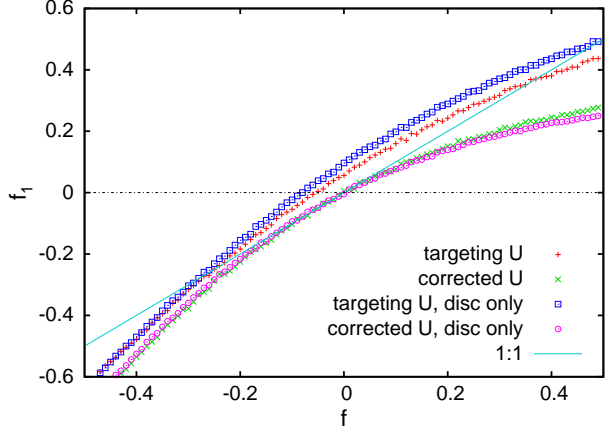


Figure 5. The effect of including the corrections for rotation of the velocity ellipsoid. Two samples are used: one has just 500 000 disc stars and the another has 450 000 disc plus 50 000 halo stars. Both samples are strongly affected by rotation of the velocity ellipsoid, yet the correction successfully shifts the points so they pass through the origin. As expected, the sample with a halo contribution is less strongly affected.

2.5.2 Correlations from random velocities

In the heliocentric frame the random component $\delta U \equiv U_0 + U_\odot - \bar{U}$ is correlated with $\delta V \equiv V_0 + V_\odot - \bar{V}$ because the velocity ellipsoid at the star's location is not aligned with that at the Sun's location, so the rotation matrix $\mathbf{R}(\alpha, \beta)$ of equation (28) is non-trivial. Consequently, when we calculate $\langle UT_{UV}V \rangle$ in the course of evaluating $\langle Ux \rangle$, the correlation will be larger than the one we want by $\langle \delta UT_{UV} \delta V \rangle$. We now determine the magnitude of this correlation so we can subtract it from the correlations we obtain from the data prior to determining f . Bearing in mind that $\langle \delta U_g \delta V_g \rangle = 0$, we have

$$\langle \delta UT_{UV} \delta V \rangle = \langle (\delta U_g \cos \alpha \cos \beta + \delta V_g \sin \alpha + \delta W_g \cos \alpha \sin \beta) \\ \times T_{UV} (-\delta U_g \sin \alpha \cos \beta + \delta V_g \cos \alpha - \delta W_g \sin \alpha \sin \beta) \rangle \quad (39) \\ = \frac{1}{4} (\cos^2 b \sin 2l \sin 2\alpha (\cos^2 \beta \sigma_U^2 - \sigma_V^2 + \sin^2 \beta \sigma_W^2))$$

Similar calculations yield the additional correlations

$$\langle \delta UT_{UW} \delta W \rangle = \frac{1}{4} \langle \sin 2\beta \sin 2b \cos l \cos \alpha (\sigma_U^2 - \sigma_W^2) \rangle \quad (40)$$

and

$$\langle \delta VT_{VW} \delta W \rangle = \frac{1}{4} \langle \sin 2b \sin l \sin \alpha \sin 2\beta (\sigma_W^2 - \sigma_U^2) \rangle \quad (41)$$

The red and blue points in Fig. 5 show what happens if one ignores the impact of azimuthal streaming and rotation of the velocity ellipsoids when determining f by plotting on the vertical axis the value of f that is recovered from equation (18) against the input value of f . The red points do not pass through the origin, so the estimated value of f is non-zero even when the distances are, in fact, correct. The green and blue points show that when the formulae above are used to subtract the contributions to the measured correlations from velocity-ellipsoid rotation, the points pass through the origin as we require. The mock data used in these tests consisted of 450 000 disc stars and 50 000 stars belonging to a non-rotating halo in one case and a pure disc sample of 500 000 objects in the other case. For one test case

only the disc stars were used, while all the stars were used in the other case.

2.6 Components with extreme velocities

Samples of halo stars generally have large mean V velocities relative to the Sun. So long as we are confident that the sample means of U_0 and W_0 are far smaller than that of V , we can greatly simplify the analysis of the sample. While some samples of high-velocity stars may show a degree of radial streaming on account of the Hercules star stream, the only indication of streaming in the vertical direction is a very small correlation between V and W that was detected in the Hipparcos proper motions by Dehnen (1998), and interpreted by him as the signature of the Galactic warp. We proceed under the assumption that $\langle U_0 \rangle = -U_\odot$ and $\langle W_0 \rangle = -W_\odot$.

At each point on the sky we imagine taking the sample mean of the third of equations (9) to obtain

$$\langle W \rangle + (1 + fT_{WV})W_\odot + fT_{WU}U_\odot = fT_{WV}\langle V_0 \rangle \quad (42)$$

On the left we neglect terms of order f and redetermine f as the value which gives the least-squares fit between the functions of sky coordinates $\langle W \rangle + W_\odot$ and $T_{WV}\langle V_0 \rangle \simeq T_{WV}\langle V \rangle$. The formal error in the recovered value is

$$\epsilon_f = \frac{1}{\sqrt{N}} \frac{\sigma_W}{\langle V \rangle \sigma_{T_{WV}}}, \quad (43)$$

where N is the number of bins on the sky. For a typical sample $\sigma_{T_{WV}} \sim 0.2$, and for halo stars we have $\langle V \rangle \sim 250 \text{ km s}^{-1}$ and $\sigma_W \sim 100 \text{ km s}^{-1}$, so $\epsilon_f \sim 2/\sqrt{N}$, which gives an error in f $\epsilon_f \simeq 6.3\%$ for a sample of 1000 objects. We can reduce this error by using the corresponding equation for $\langle U \rangle$ – the reduction is by a factor slightly smaller than $\sqrt{2}$ because $\sigma_U > \sigma_W$.

If initially our distance scale is significantly in error, our first values of $\langle V \rangle$ will be wrong. The magnitude of the problem is given by the first term on the right of the second of equations (9):

$$\langle V_0 \rangle \simeq \frac{\langle V \rangle}{1 + f\langle T_{VV} \rangle}, \quad (44)$$

where the angle brackets around T_{VV} imply the average over the surveyed region of the sky. Eliminating $\langle V_0 \rangle$ between equations (42) and (44), we obtain

$$\langle W \rangle + W_\odot \simeq \frac{f}{1 + f\langle T_{VV} \rangle} T_{WV}\langle V \rangle. \quad (45)$$

It is now straightforward to determine f from the mean slope x of the correlation between $\langle W \rangle + W_\odot$ and $T_{WV}\langle V \rangle$:

$$f = \frac{x}{1 - x\langle T_{VV} \rangle}. \quad (46)$$

This simple-minded approach to the determination of f uses the available information less efficiently than the technique described in Section 2.2, but it is a good way of detecting a systematic distance error and its sign prior to iteratively correcting the distance scale. This is the approach that led Schönrich et al. (2011) to suggest that the distances to low-metallicity stars in the SEGUE dataset were being systematically overestimated.

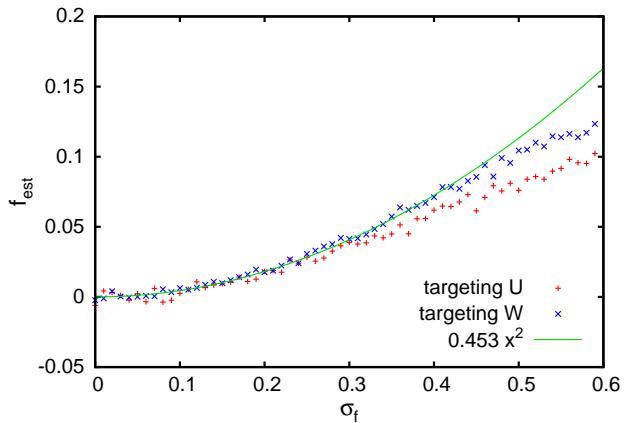


Figure 6. The effect of an unbiased Gaussian distribution of distance errors in a sample of 450 000 disc and 50 000 halo stars. For comparison we plot the fits via U and W for the corrected fitting formulae. At larger standard errors of the distances, the average distance estimate diverges quadratically. For W we show the fitting line $0.453\sigma_f^2$ obtained for $0.0 < \sigma_f < 0.4$. Beyond this point the error loses Gaussianity because we have to cut the Gaussian distribution in order to avoid negative distances.

3 SCATTER IN THE DISTANCE ERRORS

To this point we have assumed that the distances to all stars contain the same fractional error, f . In reality any systematic offset will be combined with random scatter, and we now consider whether in these circumstances the factor f that we recover from the whole population will equal the average of the f factors of the stars. In other words, does our procedure provide an unbiased estimate of f ?

3.1 The bias in f

In fact it is not hard to see from equation (18) that we must anticipate a tendency to overestimate the mean value of f : stars with $f > 0$ will be ascribed the largest velocities and will thus tend to dominate the sums implicit in $\langle Wy \rangle$ and $\langle y^2 \rangle$. From the perspective that equations (13) describe linear relations between U and x or W and y , stars with overestimated distances will dominate the ends of the line and influence more strongly our estimate of the line's slope f than stars with under-estimated distances, which will cluster near the middle of the line.

Fig. 6 shows this effect in samples of 450 000 disc and 50 000 halo stars in which the input distances have errors f that have zero mean but the dispersion σ_f that is given by the horizontal axis. The vertical axis gives the recovered value of f . To both cases we apply the corrections described in subsections 2.4 and 2.5. The expected tendency for f to be overestimated in the presence of significant scatter in the input f values manifests itself in the parabolic shape of the curves formed by the corrected results.

We can recover this behaviour analytically as follows. We assume that the stars with a given fractional distance error f' occur everywhere on the sky, so we can form the sky-average $\langle Wy \rangle_{f'}$ over just this group of stars. Defining

$$n^2 \equiv (T_{WV}^2 + T_{WU}^2)\sigma_W^2, \quad (47)$$

the inferred fractional distance error of the population is

$$f = \frac{\int f' P_f(f') \langle W y \rangle_{f'}}{\int f' P_f(f') \langle y^2 + n^2 \rangle_{f'}} = \frac{\int f' P_f(f') f' \langle y^2 \rangle_{f'}}{\int f' P_f(f') \langle y^2 + n^2 \rangle_{f'}}, \quad (48)$$

where $P_f(f')$ is the probability density function (pdf) of f' . Now we decompose $\langle y^2 \rangle$ into the part $\langle y^2 \rangle_{\perp}$ that derives from tangential velocities and the part $\langle y^2 \rangle_{\parallel}$ that derives from line-of-sight velocities. Since the inferred tangential velocities scale like $1 + f$ we then have

$$f = \frac{\int f' P_f(f') f' [(1 + f')^2 \langle y^2 \rangle_{f',\perp} + \langle y^2 \rangle_{f',\parallel}]}{\int f' P_f(f') [(1 + f')^2 \langle y^2 + n^2 \rangle_{f',\perp} + \langle y^2 + n^2 \rangle_{f',\parallel}]} \quad (49)$$

Setting $P_f \propto e^{-f^2/2\sigma_f^2}$ and neglecting the variation of $\langle y^2 \rangle_{f'}$ with f' , this yields

$$f \simeq \frac{2\sigma_f^2}{1 + \sigma_f^2 + \langle n^2 \rangle_{\perp} / \langle y^2 \rangle_{\perp} + \langle y^2 + n^2 \rangle_{\parallel} / \langle y^2 \rangle_{\perp}}. \quad (50)$$

The parabolic variation of the recovered value of f with the width σ_f of the scatter in individual f -values is now manifest.

Actually, the assumption above of a Gaussian distribution of fractional distance errors is not fully realistic. In fact, the $P_f(f)$ has a long tail at $f > 0$. Stars in this tail will have seriously overestimated tangential velocities, and Schönrich et al. (2011) argue that as a consequence a halo sample that in reality has no net rotation can be interpreted as consisting of two populations, one of which is counter-rotating.

3.2 The second moment of the error distribution

We can obtain information about the breadth of the distribution of distance errors in an approach largely similar to the classical statistic parallax: we compare the square of the speed v with the squares of the line-of-sight velocity v_{\parallel} . For the measurement of the i th star, we have

$$v_i^2 = v_{\parallel,i}^2 + F_i^2 v_{\perp,i,0}^2, \quad (51)$$

where $F_i \equiv 1 + f_i$. Summing over the N stars in the sample, we obtain

$$\begin{aligned} \frac{\overline{v^2}}{\overline{v_{\parallel}^2}} &= 1 + \frac{\sum F_i^2 v_{\perp,i,0}^2}{N \overline{v_{\parallel}^2}} \\ &= 1 + \frac{\overline{F^2} \sum v_{\perp,i,0}^2 + \sum (F_i^2 - \overline{F^2}) v_{\perp,i,0}^2}{N \overline{v_{\parallel}^2}} \\ &= 1 + \overline{F^2} \frac{\overline{v_{\perp,0}^2}}{\overline{v_{\parallel}^2}} + \frac{1}{\overline{v_{\parallel}^2}} \text{Cov} \left(F^2, \overline{v_{\perp,0}^2} \right). \end{aligned} \quad (52)$$

If the distance errors are statistically independent of velocities, the covariance vanishes. Further, if either the velocity distribution is isotropic or the sample is uniformly distributed on the sky so v_{\perp} and v_{\parallel} sample equally all three principal axes of the velocity ellipsoid, then $\overline{v_{\perp,0}^2} = 2\overline{v_{\parallel}^2}$ and equation (52) yields

$$\overline{F^2} = \frac{1}{2} \left(\frac{\overline{v^2}}{\overline{v_{\parallel}^2}} - 1 \right) \quad (\text{isotropy}). \quad (53)$$

If the velocity distribution is anisotropic and the sky coverage is non-uniform, this formula will under-estimate $\overline{F^2}$ when the sample points towards the longest axis of the velocity ellipsoid and overestimate it in the contrary case.

Classical statistical parallaxes are obtained under the assumption of isotropic velocity dispersion, which is the circumstance in which equation (53) is most likely to hold, and clearly this equation is closely related to the classical formula for a statistical parallax. The main difference is that it yields the second rather than the first moment of F .

The covariance in equation (52) is non-vanishing when the distance errors are not statistically independent of the velocities, for example, because distances are more likely to be under-estimated when looking into the plane than when looking to a Galactic pole.

In practice the scope for reliable application of equation (52) is limited since few samples are uniformly distributed on the sky and have securely known values of the covariance term.

A more effective way to determine the scatter in f exploits the idea introduced at the start of this Section that stars with overestimated distances tend to have large values of $|x|$ and $|y|$, while stars with under-estimated distances have small values of $|x|$ and $|y|$. Consequently, if in equations (18) or (19) we restrict the sum to stars with small (resp. large) x^2 or y^2 we will probe the smallest (resp. largest) values of f within the sample. By combining these estimates of f with the numbers of stars associated with each range of values of x^2 or y^2 , we can construct the probability distribution $P(f)$ of the overall sample.

Whichever approach we adopt to determine the scatter in f , we should take into account the errors in proper motions. In the first approach they increase $\overline{v_{\perp}^2}$ and $\overline{v^2}$, in the second approach they push stars to large values of x^2 and y^2 and thus affect the distance estimator. Fortunately, in relatively nearby samples the impact of errors in proper motions is limited.

4 IMPLEMENTATION

In this section we explain which of the several formulae we have given for the fractional distance error f we recommend, and in what order they should be used. Then we illustrate the procedure by applying it to a sample of stars from the Sloan Extension for Galactic Understanding and Exploration (SEGUE, Yanny et al. 2009) and a sample from Data Release 8 of the Sloan Digital Sky Survey (Eisenstein et al. 2011; Aihara et al. 2011).

In any real data set there are likely to be stars with implausibly large heliocentric velocities, and the first step should be to discard those stars. We discard stars for with extreme galactocentric velocities, i.e. $|U|, |V| > 800 \text{ km s}^{-1}$ or $|W| > 400 \text{ km s}^{-1}$. Then we bin the stars by some quantity of interest, such as surface gravity, metallicity or value of v_{ϕ} , and for each bin use equation (19) iteratively to determine f for that group. The values of $\langle W y \rangle$ used in this equation are the raw values from the data minus the corrections $\langle e_{wey} \rangle$ from equations (25) and the corrections for rotation of the velocity ellipsoid from equations (40) and (41). Once this stage in the analysis has been completed, the distances of stars have been corrected for the most im-

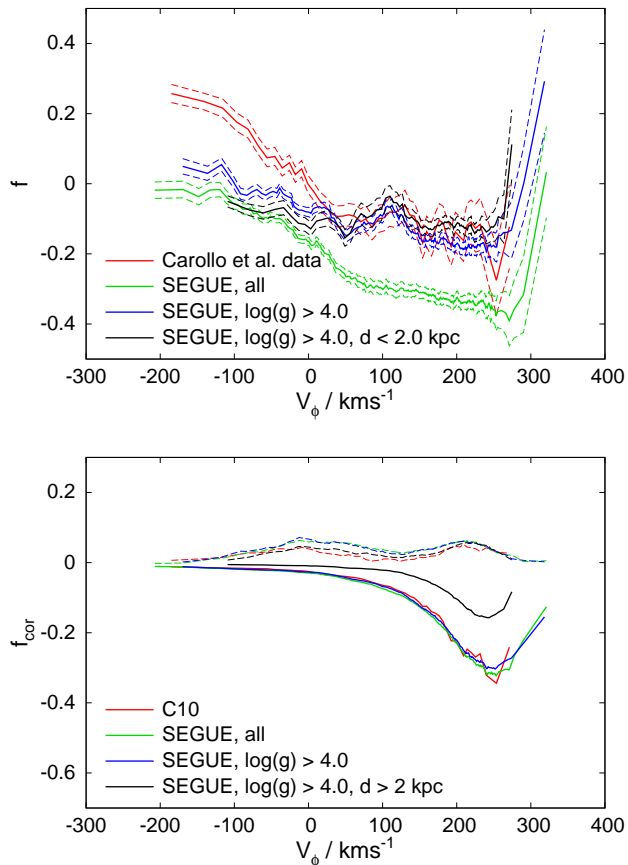


Figure 7. Values of f for the sample of $\sim 20\,000$ main-sequence stars in the sample of Carollo et al. (2010) (red curve) and three different selections on our SEGUE sample. A mask with a width of at least 1600 stars and at least 25 km s^{-1} width was moved over the sample in steps of 200 stars. The dotted lines delimit the formal 1σ error bands associated with these estimates. In the lower panel we plot the distance corrections from proper motions (negative, solid lines) and the velocity ellipsoid turn (positive, dashed lines) as defined in eq. 40.

portant errors in the original data, and we may assume that any residual systematic errors are small.

4.1 Used samples

We will make use of two subsamples from the SEGUE survey. Our main sample consists of a raw dataset of 224 019 stars from the eighth Sloan data release (DR8, Aihara et al. 2011). As we want the maximum number of stars we can get and not a specific subset and do not fear metallicity biases in the sample, we use all stars with clean photometry from target selection schemes that do not include any direct kinematic (i.e. proper motion or line-of-sight velocity) bias. To ensure decent quality of the used kinematics, we follow Munn et al. (2004) in requiring a match in the proper motion identifications ($match = 1$), a good position determination $\sigma_{RA}, \sigma_{DEC} < 350\text{ mas}$. To ensure sensible stellar parameters, we require an average signal-to-noise ratio larger than 10. Further we require the formal errors on the proper motions to be moderate: $\sigma_{\mu_b}, \sigma_{\mu_l} < 4\text{ mas yr}^{-1}$. We exclude any star that lacks a metallicity or a proper motion or is flagged

as having an unusual spectrum (Lee et al. 2008a) unless the flag indicates carbon enhancement. To eliminate a handful of objects with colours far outside the normal calibration ranges we require $0 < (g-i)_0 < 1$. Only stars that would be within 4 kpc in the first guess distance determination and pass our criteria for not being velocity outliers are used. When adopting the Ivezić et al. (2008) (A7) main-sequence distance calibration a total of 119 577 stars pass these cuts. Velocities are derived as in Schönrich et al. (2011) with an adopted solar galactocentric radius of $R_0 = 8\text{ kpc}$, a circular speed of 220 km s^{-1} and the solar motion relative to the local standard of rest from Schönrich et al. (2010). For this work we make use of the dereddened Sloan photometric colours provided in the catalogue.

The sample of Carollo et al. (2010), which comprises $\sim 30\,000$ calibration stars from SEGUE, constitutes our second sample. Its parameters derive from an earlier version (DR7, Abazajian et al. 2009) of the SEGUE parameter pipeline, but are consistent with the new data release. While their sample is no more than a mere subset of our larger sample, their sample suffers from distance overestimates (as shown by Schönrich et al. 2011) whose re-detection illustrates the potential of the method presented here.

4.2 Mapping the samples in azimuthal velocity

Fig. 7 shows the results of binning the main-sequence stars of four subsamples of SEGUE stars by azimuthal velocity v_ϕ (with the Sun at $v_\phi = 232\text{ km s}^{-1}$). The upper panel shows values of f , while the lower panel shows the corrections used to obtain these f -values.

The full lines in the bottom panel of Fig. 7 show the corrections to f that are required to account for proper-motion errors – the impact of errors in v_\parallel is negligible and not plotted. Proper-motion errors tend to increase the recovered value of f , so they require a negative correction to f . Their importance peaks around solar velocity because they contribute a roughly constant term to $\text{Cov}(W, y)$, while the typical heliocentric velocities of stars, which provide our signal, shrink as v_ϕ tends to the Sun’s value both because of the diminishing offset in the rotational component and because the velocity dispersion of disc stars diminishes as v_ϕ approaches the circular speed.

The dashed lines in the bottom panel of Fig. 7 show the corrections to f that are required to account for the rotation of the velocity ellipsoid. These curves have two peaks because there is a similar competition between decreasing heliocentric velocities and decreasing size of the velocity ellipsoid that drives the correction term.

The full red curve in the upper panel of Fig. 7 shows the values of f yielded by equation (19) when distances from Carollo et al. are used for their “main-sequence” stars; the dashed red curves show the error bounds on f . We see that f is significantly greater than zero for $v_\phi < 0$, the region of retrograde rotation, implying the presence of significant distance overestimates. At $v_\phi > 0$, f drops slightly below zero. The full green curve shows the corresponding values of f for the full SEGUE sample when distances are obtained from the Ivezić et al. (2008) (A7) main-sequence relation. Since the samples are now much larger, the formal error bounds are tighter than in the case of the Carollo et al. sample. Now at $v_\phi > 0$, f is decidedly negative (~ -0.3) implying

the presence of significant distance under-estimates. The f -value of a sample is an *average* distance correction, so a given value of f could imply that all stars have the corresponding distance mis-estimate, or that a fraction of the stars have a larger mis-estimate while the bulk of the stars have good distances. The blue full curve in the upper panel of Fig. 7 shows the values of f obtained when the all-star sample is restricted to dwarfs by imposing the restriction $\log g > 4$: with this cut the distances are under-estimated by only ~ 10 per cent because the gravity cut eliminates most sub-giants and giants from the sample. The black line shows the same “dwarf” star sample with the additional restriction for the primary distance estimate to be $d' \leq 2$ kpc. This cut removes mostly relatively blue stars that have a tendency to be on the blue side of the turn-off point. And as we can see from the black line in the lower panel the impact of proper motion errors is greatly reduced as these are proportional to the square of the estimated distance.

In light of this finding we conclude that the deep trough in the green curve for the all-star sample arises because that sample is severely contaminated by subgiants and giants. We can probe the extent of the contamination by dissecting a sample in velocity space because, as we saw in Section 3.1, stars with overestimated distances assemble at extreme velocities, while stars with under-estimated distances are dragged towards the solar motion. This is why the curves of the two contaminated samples (the Carollo et al. sample and the all-star sample) slope steeply downward from left to right in the upper panel of Fig. 7. The slope of the curve for the cleaner sample produced by the gravity cut is much smaller. We can even in analogy interpret the minor difference between the black and the blue curves: by the general inclination of the main sequence, the distance cut preferentially removes relatively bright blue stars from the sample that have a larger spread in estimated distances.

The sudden rise of f at super-solar v_ϕ has a different cause. These stars are few in number and have small heliocentric velocities, and, as the lower panel of Fig. 7 shows, their f -values are strongly affected by assumed proper-motion errors. It is likely that our probably false assumption of a constant proper-motion error has biased the f -values for these stars. By contrast, the f -values of stars with v_ϕ substantially smaller than the solar value are insensitive to the handling of proper-motion errors.

While valuable insights can be obtained by examining f as a function of velocity, a word of caution about such dissection is in order. No cut or selection should directly affect the target variable (here W), and cuts on the explaining variable can introduce artifacts that should be explored with mock data. For example cutting in the heliocentric V velocity instead of v_ϕ introduces a velocity-dependent error in f of order ~ 5 per cent. In this case the bias arises from the rotation of the velocity ellipsoid, which from selection in V creates a bias in U , which in turn evokes biases in W through the vertical tilt of the ellipsoid.

4.3 Dissecting the main sample in gravity

By partitioning a sample in gravity we can explore the extent to which a sample contains stars at different evolutionary stages since they should fall into different bins in gravity. In

the following we use only the A7 calibration of Ivezić et al. (2008).

The first three panels of Fig. 8 show results obtained by splitting the $\sim 120\,000$ stars into three ranges of metallicity, with boundaries at $[\text{Fe}/\text{H}] = -1.2$ and -0.5 and then within each metallicity group splitting the stars in $\log g$, and finally binning them in colour. Each colour bin has ≥ 1200 stars (the ones at the edges carry ≥ 800 and ≥ 400 objects), and from one bin to the next 400 stars are dropped, so every third data point is independent. Points are plotted at the average colour of the stars in the bin. Most giant stars in this sample have low measured metallicities so the low-gravity bins are only well-populated for the most metal-poor stars. The error bars indicate the formal errors on f plus an error of 30% in the corrections to f for proper-motion errors and rotation of the velocity ellipsoid.

Since the distances employed assume that every star is on the main sequence, giants have severe distance under-estimates (negative f). In the top two panels of Fig. 8 one can assess the colour at which stars move up from the sub-giant branch to the giant branch – the precision with which this colour can be determined is increased if the sample is not divided by gravity or metallicity. The distance under-estimates indicated by Fig. 8 are similar to those we would expect a priori, but the agreement is imperfect because the giants in this sample are very remote, so proper-motion errors have a big impact on kinematically determined distances.

In the literature SEGUE stars with gravities within $3.0 < \log g < 3.5$ are considered subgiants (see e.g. Carollo et al. 2010). Stars with $3.5 < \log g < 4.0$ were classified as turn-off stars until it was shown by Schönrich et al. (2011) that this practice sorts stars into unphysical positions in the colour-gravity plane (at the relevant low metallicities, the turn-off region should end bluewards of $(g-i)_0 < 0.4$). More recent studies (Beers et al. 2011; Carollo et al. 2011) classify the stars with $3.5 < \log g < 3.75$ as subgiants and the higher-gravity objects as main-sequence stars. However, the purple and blue points in the upper two panels of Fig. 8 show that it cannot be the case that all stars with $\log g < 3.75$ are subgiants, both because at $(g-i)_0 > 0.4$ the f -values of the stars with $3.5 < \log g < 3.75$ are significantly less negative than those of stars with $\log g < 3.5$, and because the f -values of the high-gravity sub-sample are no smaller than ~ -0.3 . This corresponds to their being more luminous than main-sequence stars of the same colour by less than a magnitude, whereas, depending on metallicity, already at $(g-i)_0 \sim 0.4$ subgiants should be more luminous than main-sequence stars by more than 1.5 magnitudes. We conclude that no reliable selection for subgiants is feasible with the current gravities: in general there is a contamination by dwarf stars (with the well-known effects of distance overestimates mimicking kinematically hot retrograde populations) and at least on the red side we have to expect some contamination by giants.

The main-sequence relation appears to describe relatively well the distances of stars with measured $\log g > 3.75$. Yet, especially in the top right panel of Fig. 8 we see that for all metallicity subsamples, f tends to increase bluewards. This phenomenon arises because the colour-luminosity relation we have used is inclined relative to the theoretical zero-age main sequence and assigns quite high luminosities and

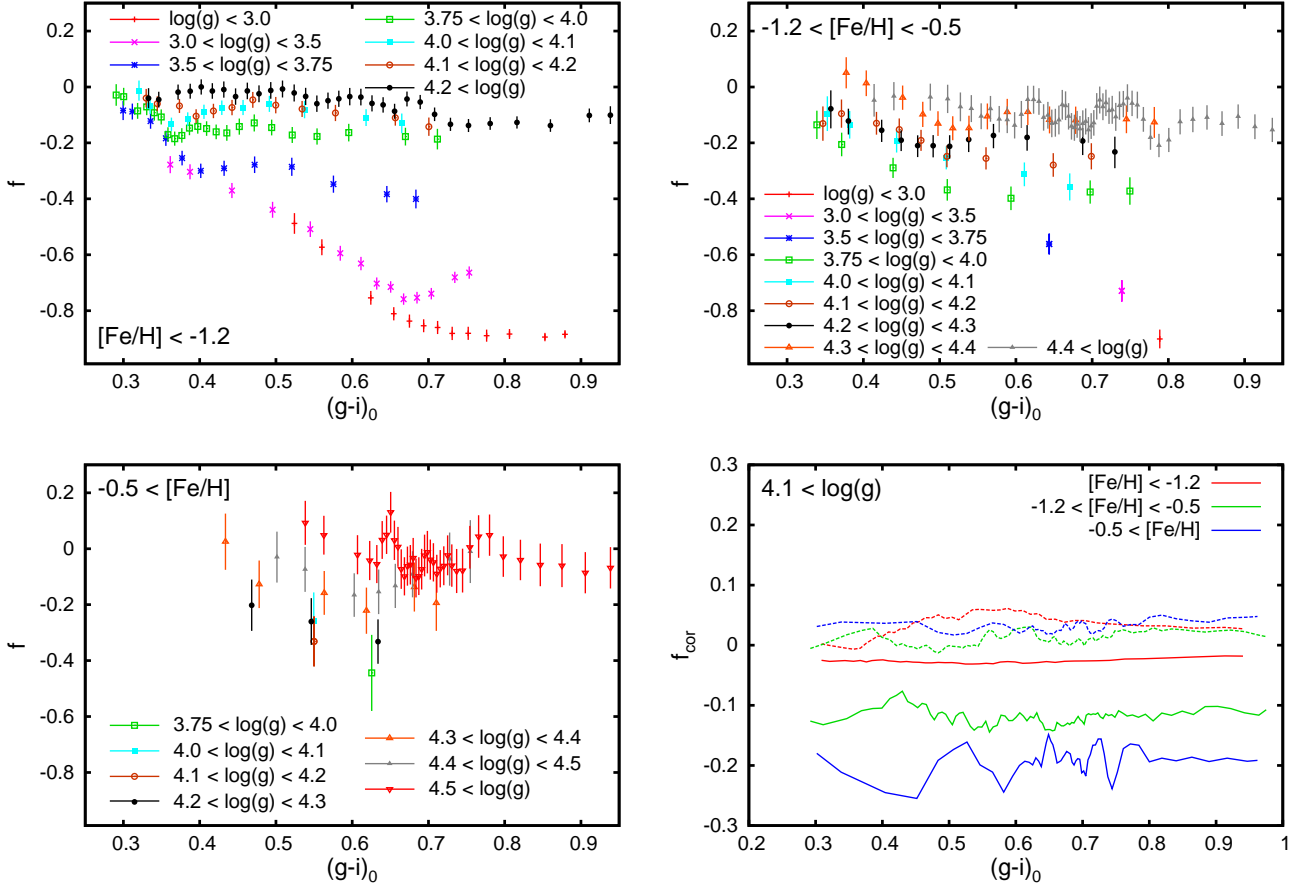


Figure 8. An evaluation of the performance of gravities in SEGUE DR8 and the performance of the Ivezić et al. (2008, A7) calibration against metallicity and colour. Each of the first three panels shows results for stars in a restricted range of metallicity. Each metallicity group was then divided by surface gravity and $g - i$ colour and f determined for that group from equation (19). We move a 1200 stars wide mask over the sample in steps of 400 objects, so that every third data point is fully independent. Error bars give the formal error plus a 30% error on the systematic corrections. The bottom right panel shows the corrections made to the f -values of high-gravity stars of various metallicities for proper motions (solid lines) and the turn of the velocity ellipsoid (dashed lines).

consequently large distances to blue stars relative to their red counterparts.

Fig. 8 enables us to choose the lower limit on gravity that will most effectively minimise contamination of the final sample by stars that are not dwarfs. This limit appears to rise from about $\log g \sim 4.1$ at the lowest metallicities to $\log g \sim 4.4$ at the highest metallicities. Some part of the trend may also be connected to the redward shift of the turn-off with metallicity. However, this conclusion should not be blindly transferred to catalogues other than DR8 because in this parameter derivation measured gravity is likely correlated with metallicity, so we may to some extent see mapping errors in assumed luminosity that arise from errors in metallicity. Fig. 8 also enables us to detect the redward shift with increasing $[\text{Fe}/\text{H}]$ in the turn-off colour as the colour at which the dark-blue points of lower-gravity stars become clearly separated from the black points of dwarf stars. Also, blueward of the turn-off we expect an increased spread in values of f within the highest-gravity bins, as the SEGUE stellar parameter pipeline retains some residual information on how high above the main sequence a star is placed in gravity.

The bottom-right panel of Fig. 8 shows the corrections to f required by proper-motion errors (solid lines) and rotation of the velocity ellipsoid (dashed lines). The impact of proper-motion errors on the most metal-weak stars is small because these stars are in the halo and have large heliocentric velocities. Rotation of the velocity ellipsoid has similar impact on stars of all metallicities because these stars are distributed through broadly the same volume and a higher velocity dispersion both inflates the correction and the signal in f . For this plot velocity errors were calculated by measuring the dispersions in each subsample and then assuming constant velocity dispersions in the lowest metallicity bin and in the other metallicity bins an increase of the dispersion by 15 per cent for each kiloparsec in $|z|$ and assuming that $\langle U^2 \rangle^{1/2} \propto \exp(-R/R_\sigma)$ with $R_\sigma = 7.5$ kpc. This correction term is small and minor changes in how it is derived will not alter our results.

5 CONCLUSIONS

Systematic distance errors give rise to correlations between the measured components (U, V, W) of heliocentric veloc-

ities. Similar correlations arise from three other sources: (i) measurement errors in the proper motions, (ii) Galactic streaming motions and (iii) dependence of the orientation of the local velocity ellipsoid on position in the Galaxy. However, each of these sources of correlation between (U, V, W) has a different and known pattern of variation over the sky, so provided the data come from a wide-area survey, we can disentangle their effects. We have described an iterative procedure by which the distances to stars are rescaled until correlations between (U, V, W) are fully accounted for by effects (i) – (iii) above, and the contribution from systematic distance errors vanishes.

The procedure works best when the group of stars under study has a large net motion with respect to the Sun. This net motion is often dominated by azimuthal streaming, since the Sun has more angular momentum than a circular orbit, while nearby thick-disc and halo stars tend to have substantially less angular momentum. When azimuthal streaming is dominant, the simpler formulae of Section 2.6 apply. For stars in the thin disc that have similar angular momentum to that of the Sun the other velocity components usually still carry sufficient information to assess distances.

In principle we can determine distance errors by using either U , V or W as a “target” variable, with the “explaining” variable being composed of the other components of velocity and the sky coordinates. In practice V should not be used as a target variable as the systematic variation of V velocities with position in the Galaxy would invoke spurious correlations with the angle terms connecting it to the explaining velocity components. W is the target variable of choice both because it has the smallest velocity dispersion and because it is least affected by the complexities of differential rotation. U is mainly useful as a target variable for its ability to determine the mean rotation rate of a population once the distance scale has been corrected by exploiting W . We will discuss an application to this rotation term in a forthcoming paper.

There are some restrictions on the applicability of the method that should be borne in mind when using it. The proper motions need to be unbiased and their errors should have finite and approximately known variances. These conditions seem to be satisfied by data from the SDSS (Dong et al. 2011). If the sample is non-local we need to estimate the extent of rotation of the velocity ellipsoid within the sampled region. Such an estimate can be obtained from the sample itself, but with some residual uncertainty arising from proper-motion errors that particularly affect remote stars.

Streams and a warp will induce unwanted correlations but the likelihood of these giving rise to an erroneous distance scale is small for several reasons. First, for a stream or warp to undermine the method, the correlations it introduces must vary on the sky in a similar way to the correlations associated with distance errors. Consequently, the impact of a stream or warp is likely to be suppressed given sufficient sky coverage. Second, a warp could be accounted for in much the same way we have accounted for Galactic rotation. Third, the footprints of streams or a warp will show up in conflicting values for f obtained from the two possible target velocities, W and U . Finally, a stream or warp would induce identical correlations in the velocities of stars in the broad colour and gravity range that made up the physi-

cal feature, whereas distance mis-estimates will usually vary with spectral type.

In Section 3.1 we showed that the estimators given in Section 2 are mildly biased in the sense that when there is a scatter in the distribution of distance errors, the estimated value of f will be larger than it should be by an expression quadratic in the width of the distribution. Equation (50) can be used to correct for this effect. As we discussed in Section 3.2, the method can be extended to probe the full probability distribution of f values rather than just determining the mean value of f . Details of this extension will be given in a later paper.

In Section 4 we applied the method to samples of stars from the SEGUE survey. We concluded that the distances to stars used by Carollo et al. (2010) are on average significantly overestimated among stars deemed to be counter-rotating, and tend to be under-estimated by ~ 10 per cent near solar velocity. This is also a nice example on how a spread in the distance errors within a sample can be directly seen by eye, when we dissect the sample in velocity: the distance overestimates assemble at velocities remote from the solar value (i.e. mostly the retrograde tail of the halo velocity distribution), while in our all-star sample, which is contaminated by numerous giants, the giants are dragged towards the solar motion, so a trough forms in a plot of the correction factor f versus azimuthal velocity. We also warn against mistaking the derived values for a direct estimate of absolute magnitudes. Apart from contaminations the method corrects for the mean reddening error and the presence of unresolved binaries. So in general it can be expected to give slightly larger mean distances than appropriate for single stars.

In Section 4.3 we demonstrated the use of the method to assess the reliability of the Ivezić (2008) A7 distance scale for dwarfs and to assess the degree of contamination by non-dwarfs that arises as the lower limit on $\log g$ for entering the sample is varied. For low contamination the lower limit on $\log g$ should increase with metallicity. We conclude that using only the DR8 gravities it is not possible to achieve a satisfying selection of subgiants. The level of contamination by dwarf stars becomes large once the upper limit on $\log g$ exceeds ~ 3.5 . Since any dwarf that is misidentified as a subgiant has a seriously overestimated distance, studies of stellar kinematics that are based on DR8 gravities should rigorously exclude subgiants.

We are currently applying the method to recent distances to stars in the RAVE survey (Zwitter et al. 2010; Burnett et al. 2011). A wide variety of applications to this method will follow as it offers a standard tool to identify groups of stars with problematic parameters, to check the reliability of selection schemes and distance assignments and finally to correct for any biases in these distances, e.g. by deviations in reddening with distance from the Sun.

Our study has also illuminated the kinematic patterns that distance errors can generate. These are not limited to the production of spurious counter-rotating components, but include tilts of the velocity ellipsoids, and by allowing rotational velocity to masquerade as motion in either the radial or vertical direction, can extend to patterns of mean motion that, in a sample that is anisotropically distributed on the sky, can imply a wrong motion of the local standard of rest.

ACKNOWLEDGEMENTS

R.S. acknowledges financial and material support from Max-Planck-Gesellschaft. We thank Michael Aumer for the kind provision of his galaxy models and Ruobing Dong for helpful discussions on SDSS proper motions. We thank M. Williams for careful reading and comments.

REFERENCES

- Abazajian K. et al., 2009, *ApJS*, 182, 543
 Aihara H. et al., 2011, *ApJS*, 193, 29
 Beers T.C. et al., 2011, arXiv:1104.2513
 Binney, J., McMillan P.J., 2011, *MNRAS*, 413, 1889
 Binney J., Merrifield M., 1998, “Galactic Astronomy”,
 Princeton: Princeton University Press
 Burnett B., and the RAVE collaboration, *A&A*, 523, 113
 Carollo D. et al., 2010, *ApJ*, 712, 692
 Carollo D. et al., 2011, arXiv:1103.3067
 Casagrande L., Flynn C., Portinari L., Girardi L., Jimenez
 R., 2007, *MNRAS*, 382, 1516
 Casagrande L., Schönrich R., Asplund M., Cassisi S.,
 Ramírez I., Meléndez J., Bensby T., Feltzing S., 2011,
A&A, 530, 138
 Dehnen, W., 1998, *AJ*, 115, 2384
 Dong R., Gunn J., Knapp G., Rockosi C., Blanton M.,
 2011, *AJ*, 142, 116
 Eisenstein D. et al., 2011, *AJ*, 142, 72
 Holmberg J., Nordström B., Andersen J., 2007, *A&A*, 475,
 519
 Ivezić Ž. et al., 2008, *ApJ*, 684, 287
 Lee Y.S. et al., 2008, *AJ*, 136, 2022
 Lee Y.S. et al., 2008, *AJ*, 136, 2050
 Lutz T.E., Kelker D.H., 1973, *PASP*, 85, 573
 Munn J.A et al., 2004, *AJ*, 127, 3034
 Nordström B. et al., 2004, *A&A*, 418, 989
 Percival S., Salaris M., 2009, *ApJ*, 703, 1123
 Popowski P., Gould A., 1998, *ApJ*, 506, 259
 Schönrich R., Binney J., Dehnen W., 2010, *MNRAS*, 403,
 1829
 Schönrich R., Asplund M., Casagrande L., 2011, *MNRAS*,
 415, 3807
 Siebert A., et al., 2011, RAVE DR3
 Trumpler R.J., Weaver H.F., 1962, *Statistical Astronomy*,
 New York, Dover Publications
 White H., 1980, *Econometrica*, 48, 817
 Yanny B. et al., 2009, *AJ*, 137, 4377
 Zwitter T., & the RAVE collaboration, 2010, *A&A*, 522,
 54